Dalton Transactions

PAPER

View Article Online
View Journal | View Issue

Cite this: *Dalton Trans.*, 2015, **44**, 13250

Metal loading of lanthanidopolymers driven by positive cooperativity†

Thi Nhu Y Hoang, Zheng Wang,‡ Lucille Babel, Homayoun Nozary, Michal Borkovec, Istvan Szilagyi* and Claude Piguet*

Received 16th May 2015,
Accepted 22nd June 2015

DOI: 10.1039/c5dt01842k

www.rsc.org/dalton

This work demonstrates how the thermodynamic loading of monodisperse polymeric single-stranded multi-tridentate receptors of variable lengths is controlled by the nature of the metallic carrier Ln(hfac)$_3$ (Ln is La, Eu or Y, and hfac is hexafluoroacetylacetonate). Whereas the intrinsic affinity of the tridentate binding site is maximum for medium-sized Eu^{3+} and decreases for Y^{3+}, the contraction of the hydrodynamic radius of the polymer upon metal loading induces positive allosteric cooperativity for the smaller cations. The origin of this behaviour is rationalized within the frame of intermetallic dipole–dipole interactions modulated by the solvation potential of dipolar solutes in dielectric materials. Positive cooperativity produces local high-density of metal ions along the ligand strands (metal clustering) with potential interest in energy migration and sensing processes.

Introduction

Wolf-type II metallopolymers correspond to rigid multi-site receptors **L**, to which the metallic units **M** closely interact with their backbone upon complexation (Fig. 1).[1] Assuming that (i) the intersite separation remains essentially invariant during the stepwise intermolecular reactions leading to the microspecies $\{\boldsymbol{s_i}\}$-[M_m**L**] (eqn (1), $\{\boldsymbol{s_i}\}$ is a state vector testifying to the exact location of each metal in the associated microspecies, and for which each element $s_i = 1$ when a metal is bound to site i and $s_i = 0$ when no metal is coordinated) and (ii) the intermetallic interactions are restricted to nearest-neighbour interactions, the associated free energy change of complexation $\Delta G^{M,L}_{m,1}\{\boldsymbol{s_i}\}$ only depends on the non-cooperative intrinsic affinity of site i for the entering metal $\Delta G^{M}_{i} = -RT(f^{M}_{i})$ and the free energy of interaction $\Delta E^{M,M}_{i,j}$ occurring when two adjacent sites i and j are occupied (Fig. 1).[2]

$$\mathbf{L} + m\mathbf{M} \rightleftharpoons \{\boldsymbol{s_i}\}\text{-}[\mathbf{M}_m\mathbf{L}] \quad \beta^{M,L}_{m,1}\{\boldsymbol{s_i}\} \qquad (1)$$

The associated binding isotherms[3] predict that larger metal-binding site affinities f^{M}_{i} reduce the concentration of free metal required for the quantitative loading of the polymer (Fig. 2a). This trend is further enhanced by the operation of positive allosteric cooperativity ($\Delta E^{M,M}_{i,j} < 0$, Fig. 2b).[4] Please note that positive cooperativity is accompanied by metallic clustering during the loading process, a phenomenon which locally increases the density of metals and finds applications in sensing[5] and in controlling intermetallic energy migration processes with emissive trivalent lanthanide cations.[6] The reverse situation holds for anti-cooperativity ($\Delta E^{M,M}_{i,j} > 0$) with the appearance of an intermediate plateau around $\theta_M = 0.5$ where the speciation is dominated by the microspecies with alternating metal-free and metal-occupied sites (Fig. 2b).[4]

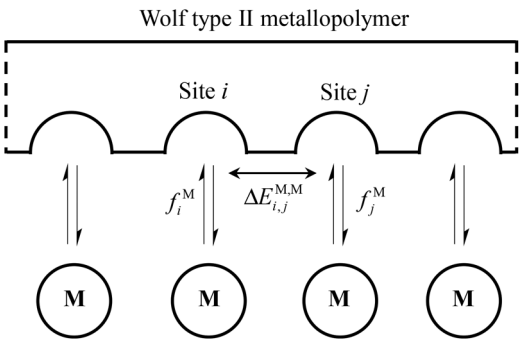

Fig. 1 Thermodynamic model for the successive intermolecular connections of metallic units to a one-dimensional multi-site receptor **L** possessing N available binding sites. f^{M}_{i} and $\Delta G^{M}_{i} = -RT\ln(f^{M}_{i})$ are the non-cooperative intrinsic affinity, respectively free energy of connection of site i for the entering metal and $\Delta E^{M,\ M}_{i,j}$ is the free energy of interaction occurring when two adjacent sites i and j are occupied.

Department of Inorganic and Analytical Chemistry, University of Geneva, 30 quai E. Ansermet, CH-1211 Geneva 4, Switzerland. E-mail: Claude.Piguet@unige.ch, Istvan.Szilagyi@unige.ch

†Electronic supplementary information (ESI) available: Table of synthetic optimization and figures showing gel permeation chromatography traces, static and dynamic light scattering measurements, ^{1}H and ^{19}F NMR spectra, binding isotherms and polymer purification. See DOI: 10.1039/c5dt01842k

‡Current address: Ministry-of-Education Key Laboratory for the Synthesis and Application of Organic Functional Molecules, College of Chemistry and Chemical Engineering, Hubei University, Wuhan 430062, P. R. China.

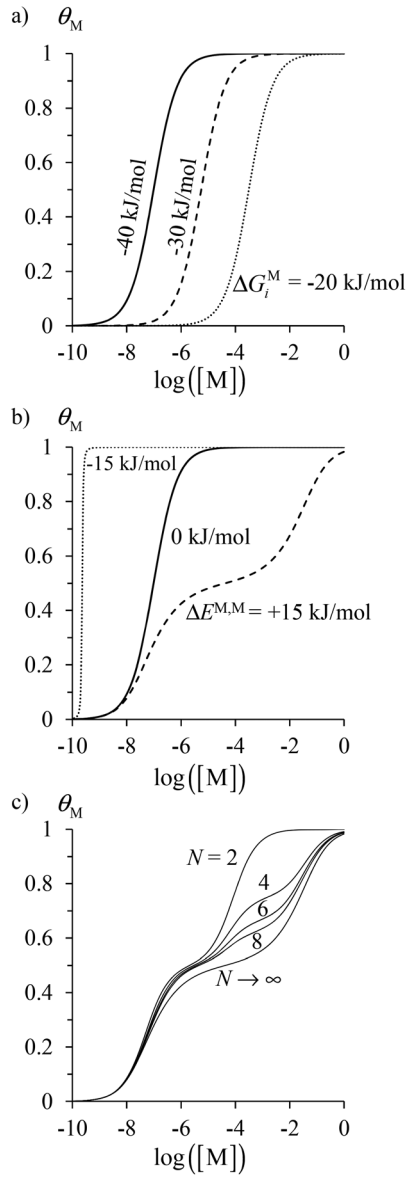

Fig. 2 Binding isotherms computed with eqn (9) and (10) for the metal loading of a linear polymer **L** with N binding sites showing the influence of (a) the intrinsic metal–ligand affinity $\Delta G_i^M = -RT(f_i^M)$ for $N \to \infty$, (b) the nearest neighbour interaction $\Delta E_{i,j}^{M,M}$ for $N \to \infty$ (ΔG_i^M = −40 kJ mol^{-1} is fixed) and (c) the number of available binding sites (ΔG_i^M = −40 kJ mol^{-1} and $\Delta E_{i,j}^{M,M}$ = 15 kJ mol^{-1} are fixed).

Again, luminescent lanthanidopolymers may benefit from this special arrangement for the detection of gases in the empty sites,[7] for the speciations of biologically relevant analytes,[8] and for the implementation of energy-transfer upconversion processes where each activator (usually an Er^{3+} cation) requires two neighbouring metallic sensitizers (usually Yb^{3+} cation).[9] However, the deliberate implementation of these thermodynamic recognition process remains unattainable at the molecular level for pairs of different lanthanide cations[10] and upconverting f–f′ systems are currently limited to statistically doped ionic solids and nanomaterials.[9]

To the best of our knowledge, a very limited number of Wolf-type-II metallopolymers coded for lanthanide loading have been identified and reported,[11] among which only three multi-site polydisperse receptors **L1**,[12] **L2**[13] and **L3**[14] include tridentate binding units, which are able to saturate the coordination spheres of hexacoordinated lanthanide nitrates ($Ln(NO_3)_3$) and lanthanide hexyfluoroacetylacetonates ($Ln(hfac)_3$) in the final lanthanidopolymers $[\mathbf{Lk}(LnX_3)_m]$ (Scheme 1).

Whereas $[\mathbf{L1}(TbCl_3)_m]$[12] and $[\mathbf{L2}(Eu(NO_3)_3)_m]$[13] were prepared by mixing the polymeric receptors with metallic salts under non-stoichiometric conditions for a rough investigation of the optical and liquid crystalline properties of the resulting solid materials, the thermodynamic loading of $[\mathbf{L3}(Ln(hfac)_3)_m]$ in dichloromethane with Ln = La, Eu and Y showed minor anti-cooperative intermetallic interactions ($0 \leq \Delta E_{1-2}^{Ln,Ln} \leq 1.4$ kJ mol^{-1}), which were too small to induce selective binding at room temperature.[14] A rational tuning of the intermetallic interactions $\Delta E_{1-2}^{Ln,\,Ln}$ is tricky because, except for melting processes occurring in condensed phases,[15] the intermolecular association reaction depicted in eqn (1) strongly depends on solvation effects.[16] This lead Choppin[17] to consider any complexation process as the result of the two successive equilibria (2) and (3), where S are solvent molecules.

$$[\mathbf{L}(S)_y]^{z-} + m[Ln(S)_x]^{3+} \rightleftharpoons [\mathbf{L}(S)_{y-q}]^{z-} + m[Ln(S)_{x-p}]^{3+} + (p+q)\ S \quad \Delta G_{desolv}^{Ln,\mathbf{L}} \tag{2}$$

$$[\mathbf{L}(S)_{y-q}]^{z-} + m[Ln(S)_{x-p}]^{3+} \rightleftharpoons [Ln_m(\mathbf{L})(S)_{x+y-p-q}]^{(3-z)+} \quad \Delta G_{asso}^{Ln,\mathbf{L}} \tag{3}$$

Since the global free energy change $\Delta G_{m,1}^{Ln,\mathbf{L}}(\{\boldsymbol{s_i}\}) = \Delta G_{desolv}^{Ln,\mathbf{L}} + \Delta G_{asso}^{Ln,\mathbf{L}}$ represents the sum of two opposite contributions,[17]

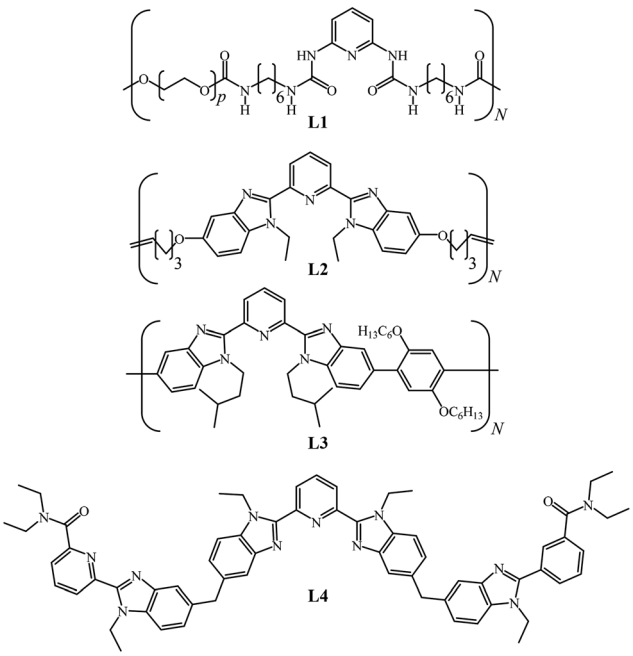

Scheme 1 Chemical structures of the ligands **L1**–**L4**.

there is no doubt that the microscopic parameters $\Delta G_i^{Ln} = -RT(f_i^{Ln})$ and $\Delta E_{1-2}^{Ln,Ln}$ similarly reflect the competition between solvation effects and intermetallic electrostatic interactions.[18] Consequently, the prediction of the magnitude and even of the sign of $\Delta E_{i,j}^{Ln,Ln}$ proved to be elusive,[19] an assertion illustrated by the opposite trend found for the loading of the oligomeric ligand **L4** which is anticooperative with $Ln(NO_3)_3$ ($\Delta E_{1-2}^{Ln,Ln} > 0$) and cooperative with $Ln(hfac)_3$ ($\Delta E_{1-2}^{Ln,Ln} < 0$, Scheme 1).[20] Since the solvation energies of charged molecules, modeled with Born eqn (4),[21] or of neutral dipolar molecules, modeled with Onsager eqn (5)[22] depend on some power of the inverse of their ionic radius R^{-k}, we reasoned that an increase in the polymer length (and size) might have significant influence on the cooperativity of the lanthanide loading. In eqn (4) and (5), $N_{Av} = 6.023 \times 10^{23}$ mol^{-1} is Avogadro's number, z is the charge of the particle in electrostatic units, $e = 1.602 \times 10^{-19}$ C is the elementary charge, $\varepsilon_0 = 8.859 \times 10^{-12}$ C^2 N^{-1} m^{-2} is the vacuum permittivity, ε_r is the relative dielectric permittivity, μ is the dipole moment of the particle and R_i is the pseudo-spherical radius of the charged ion for eqn (4) and the radius of a spherical cavity cut from the dielectric when a spherical solute is immersed into the solvent for eqn (5).

$$\Delta_{solv}G^\circ = -N_{av}\frac{z^2e^2}{8\pi\varepsilon_0 R_i}\left(1-\frac{1}{\varepsilon_r}\right) \quad (4)$$

$$\Delta_{solv}G^\circ = -N_{av}\frac{\mu^2}{4\pi\varepsilon_0 (R_i)^3}\left(\frac{\varepsilon_r-1}{2\varepsilon_r+1}\right) \quad (5)$$

We report here on the preparation of linear monodisperse multi-tridentate polymers **L3**^{N} ($10 \le N \le 30$) of increasing sizes, which are reacted with neutral dipolar $Ln(hfac_3)_m$ lanthanide carriers (Ln = La, Eu and Y). The formation of the resulting lanthanidopolymers [**L3**^{N}(Ln(hfac)$_3$)$_m$] is monitored either by ^{1}H- or by ^{19}F-NMR for extracting the thermodynamic parameters, while Dynamic Light Scattering (DLS) is used for addressing the hydrodynamic diameter in dichloromethane solutions. A special emphasis is put on the correlations between the change in hydrodynamic diameter of the lanthanidopolymers [**L3**^{N}(Ln(hfac)$_3$)$_m$] upon metal loading and the sign and magnitude of the intermetallic interactions $\Delta E_{1-2}^{Ln,Ln}$.

Results and discussion

Synthesis and characterization of the polymeric multi-tridentate receptors L3^N

The receptors **L3**^{N} are obtained by Suzuki-type coupling reactions between 2,6-bis-[1-(3-methylbutyl)-5-bromo-benzomidazol-2-yl)pyridine (**1**)[23] and 2,5-dihexyloxy-1,4-diboronic acid (**2**)[24] in the presence of $Pd(PPh_3)_4$ as catalyst and CsF as base (Scheme 2).[25] Polymerization is stopped by the successive addition of bromobenzene and phenylboronic acid, which act as terminating agents. Depending on the solvent used, the reaction time and the concentration of the reactants, the degree of polymerization, as estimated by the weight average molecular weight M_w deduced from gel permeation chromatography (GPC), varies by a factor three ($7500 \le M_w \le 22\,000$ g mol^{-1}), while the polydispersity indexes $I_p = M_w/M_n$ span the 1.03–1.6 range (M_n is the number average molecular weight, Table S1 in the ESI†). In order to prepare sufficient quantities of three different oligomers with N values stepwise incremented by approximately ten units (Table 1), we performed large scale reactions under the empirical conditions identified (Table S1†) for the preparation of monodisperse **L3**$^{N=12}$ (dioxane/ethanol (3 : 1); I_p = 1.13), **L3**$^{N=20}$ (dioxane/ethanol (3 : 1); I_p = 1.16), and **L3**$^{N=31}$ (toluene/ethanol (3 : 1); I_p = 1.25). Gel permeation chromatography (GPC) in tetrahydrofuran displayed symmetrical traces compatible with narrow distributions of the oligomers around their weight average molecular weight M_w (Fig. S1 in the ESI†), a value which is used for estimating the number of repeating units by using eqn (6) (M_0 = 726 g mol^{-1} is the molecular weight of a repeating unit and ew = 77 g mol^{-1} is the excess molecular weight brought by the terminating agent approximated as one phenyl ring, Table 1).[14]

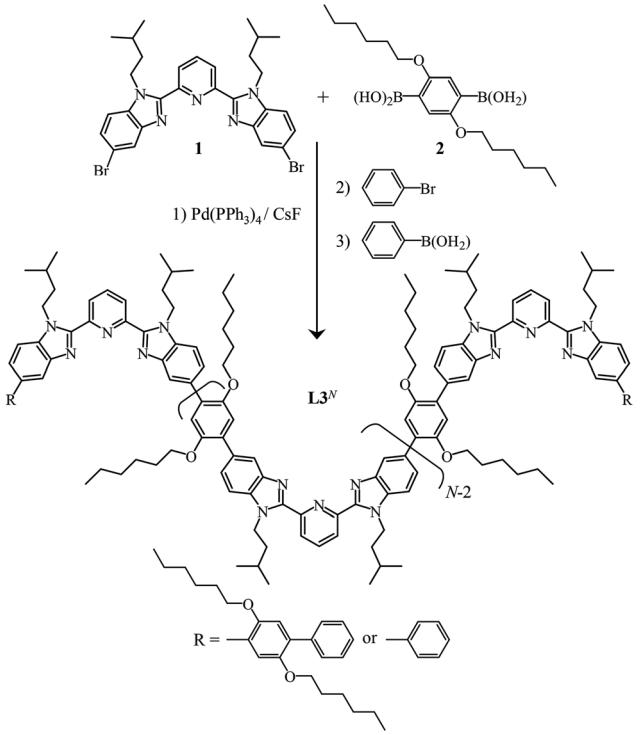

Scheme 2 Syntheses of the multi-tridentate polymeric receptors L3^N.

$$N_w = \frac{M_w - ew}{M_0} \quad (6)$$

Concentration-dependent static light scattering (SLS) experiments performed on dichloromethane solutions of the three polymers **L3**$^{N=12}$, **L3**$^{N=20}$ and **L3**$^{N=31}$ yielded similar molecular weights as the GPC method (Table 1 and Fig. S2 and S3†). For **L3**$^{N=12}$, the molecular weight is probably underestimated by SLS since one works close to detection limit of our setup. Finally, the ^{1}H NMR spectra of **L3**$^{N=12}$, **L3**$^{N=20}$ and **L3**$^{N=31}$ point to the expected alternation of one phenyl spacer with one tri-

Table 1 Weight average (M_w) and number average (M_n) molecular weights and polydispersity indexes $I_p = M_w/M_n$ for $\mathbf{L3}^N$ (N = 12, 20, 31) measured by gel permeation chromatography (GPC in THF, 303 K) and by static light scattering (SLS in CH_2Cl_2, 298 K)

Method	GPC	GPC	GPC	GPC	SLS	SLS
Polymer	M_w/g mol^{-1}	M_n/g mol^{-1}	N_w (eqn (6))	I_p	M_w/g mol^{-1}	N_w (eqn (6))
$\mathbf{L3}^{N=12}$	8743(175)	7711(154)	12	1.13(3)	4666(285)	6
$\mathbf{L3}^{N=20}$	14 759(295)	12 685(250)	20	1.16(3)	16 100(338)	22
$\mathbf{L3}^{N=31}$	22 456(450)	17 993(350)	31	1.25(4)	20 200(2980)	28

dentate binding along the strand, thus leading to a ratio for the integrated diagnostic signals close to 1.0 (Fig. S4 in the ESI†), in agreement with the structure of the polymer $\mathbf{L3}^N$ depicted in Scheme 2.

Thermodynamic loading of the polymeric multi-tridentate receptors $\mathbf{L3}^N$ with [Ln(hfac)$_3$(diglyme)]

Theoretically, the free energy change $\Delta G^{M,L}_{m,1}\{s_i\}$ accompanying the complexation of a multi-site receptor **L** in the microspecies $\{s_i\}$-[M$_m$**L**] (equilibrium (1) and Fig. 1) is given by eqn (7), where f_i^M corresponds to the non-cooperative intrinsic affinity of site i for the entering metal and $\Delta E^{M,M}_{i,j}$ stands for the free energy of interaction occurring when two adjacent sites i and j are occupied.[2]

$$\Delta G^{M,L}_{m,1}(\{s_i\}) = -\sum_{i=1}^{N} RT\ \ln\left(f_i^M\right)s_i + \frac{1}{2}\sum_{i=1}^{N}\sum_{j\neq i}^{N}\Delta E^{M,M}_{i,j}s_i s_j \qquad (7)$$

Application of the vant'Hoff equation transforms the free energy change $\Delta G^{M,L}_{m,1}\{s_i\}$ into the formation constant $\beta^{M,L}_{m,1}\{s_i\}$ for each microspecies $\{s_i\}$-[M$_m$**L**] (eqn (8)). The combination of all the microconstants possessing the same total number m of bound metals ultimately gives the target macroconstant $\beta^{M,L}_{m,1} = \sum_{\{s_i\}}\beta^{M,L}_{m,1}\{s_i\}$, which is familiar to coordination chemists.

$$\beta^{M,L}_{m,1}\{s_i\} = \prod_{i=1}^{N}\left(f_i^M\right)^{s_i}\sqrt{\prod_{i=1}^{N}\prod_{j\neq i}^{N}\left[\exp\left(-\Delta E^{M,M}_{i,j}/RT\right)\right]^{s_i s_j}} \qquad (8)$$

By computing the semigrand partition function Ξ, one can deduce the macroconstants $\beta^{M,L}_{m,1}$ of a linear polymer possessing N binding sites from f_i^M and from the Boltzmann factor representing the intercomponent interaction $u^{M,M}_{i,j} = \exp(-\Delta E^{M,M}_{i,j}/RT)$ with the matrix transfer formalism according to eqn (9), where ${}^TV_t = (1\ \ 1\ \ \ldots\ \ 1)$ and ${}^TV_g = (1\ \ 0\ \ \ldots\ \ 0)$ are the transposed terminating and generating vectors, respectively.[2]

$$\Xi = \sum_{m=0}^{N}\beta^{M,L}_{m,1}[M]^m = {}^TV_t\begin{pmatrix}1 & 1\\ f_i^M[M] & f_i^M u^{M,M}[M]\end{pmatrix}^N V_g \qquad (9)$$

The degree of metalation $\theta_M = \langle m\rangle/N$, better known in coordination chemistry as the occupancy factor, which corresponds to the average of bound metal per binding site, is related to the binding polynomial $\Xi = \sum_{m=0}^{N}\beta^{M,L}_{m,1}[M]^m$ by a simple derivative in eqn (10).

$$\theta_M = \frac{\langle m\rangle}{N} = \frac{1}{N}\frac{|M_{bound}|}{|L_{tot}|} = \frac{1}{N}\frac{d\ln(\Xi)}{d\ln([M])} = \frac{1}{N}\frac{\sum_{m=0}^{N} m\beta^{M,L}_{m,1}([M])^m}{\Xi} = \frac{1}{N}\frac{\sum_{m=0}^{N} m\beta^{M,L}_{m,1}([M])^m}{\sum_{m=0}^{N}\beta^{M,L}_{m,1}([M])^m} \qquad (10)$$

Experimentally, the titrations of the polymers $\mathbf{L3}^N$ with [Ln(hfac)$_3$dig] (Ln = La, Eu, Y; hfac = hexafluoroacetylacetonate, dig = diglyme = 1-methoxy-2-(2-methoxyethoxy)ethane)[26] were conducted in dichloromethane containing a fixed concentration of diglyme ([dig]$_{tot}$ = 0.15 mol dm^{-3}) and monitored by ^{1}H-NMR (Ln = La, Y; Fig. 3) and ^{19}F-NMR at 293 K (Ln = Eu; Fig. S5 in the ESI†). In these conditions, the ligand exchange equilibria (11) reduce to conditional stability constants $\beta^{Ln,L3^N}_{m,1,cond}$ (eqn (12)), which are adapted for being analysed within the frame of the site-binding model with the help of eqn (7)–(10).[14] Since no significant dissociation of the metallic salts occurs in dichloromethane at submillimolar concentrations,[14] [Ln(hfac)$_3$(dig)] exists as a single species in solution during the NMR titrations, the concentration of which is written as [Ln] for the rest of this work.

$$\mathbf{L3}^N + m[Ln(hfac)_3(dig)] \rightleftharpoons [\mathbf{L3}^N(Ln(hfac)_3)_m] + m dig$$

$$\beta^{Ln,L3^N}_{1,m} = \frac{[\mathbf{L3}^N(Ln)_m][dig]^m}{[Ln]^m[\mathbf{L3}^N]} \qquad (11)$$

$$\beta^{Ln,L3^N}_{m,1,cond} = \frac{\beta^{Ln,L3^N}_{m,1}}{([dig]_{tot})^m} = \frac{[\mathbf{L3}^N(Ln)_m]}{[Ln]^m[\mathbf{L3}^N]} \qquad (12)$$

For each point of the titration, the NMR spectra are recorded at thermodynamic equilibrium and the intensity of signals of a given nucleus (*e.g.*, proton), neighboring to the free tridentate site (I^H_P) can be compared with that of the same nucleus, but connected to a bound site (I^H_{P-Ln}). Since the total concentration of metal [Ln]$_{tot}$ and of polymer [$\mathbf{L3}^N$]$_{tot}$ is known at each point of the titration, the amount of bound [Ln]$_{bound}$ (eqn (13)) and free [Ln] (eqn (14)) metal are experimentally accessible together with the degree of metalation θ_{Ln} (eqn (15)) plotted in Fig. 4 and Fig. S6 (in the ESI†).[27]

$$[Ln]_{bound} = \left(\frac{I^H_{P-Ln}}{I^H_P + I^H_{P-Ln}}\right)N[\mathbf{L3}^N]_{tot} \qquad (13)$$

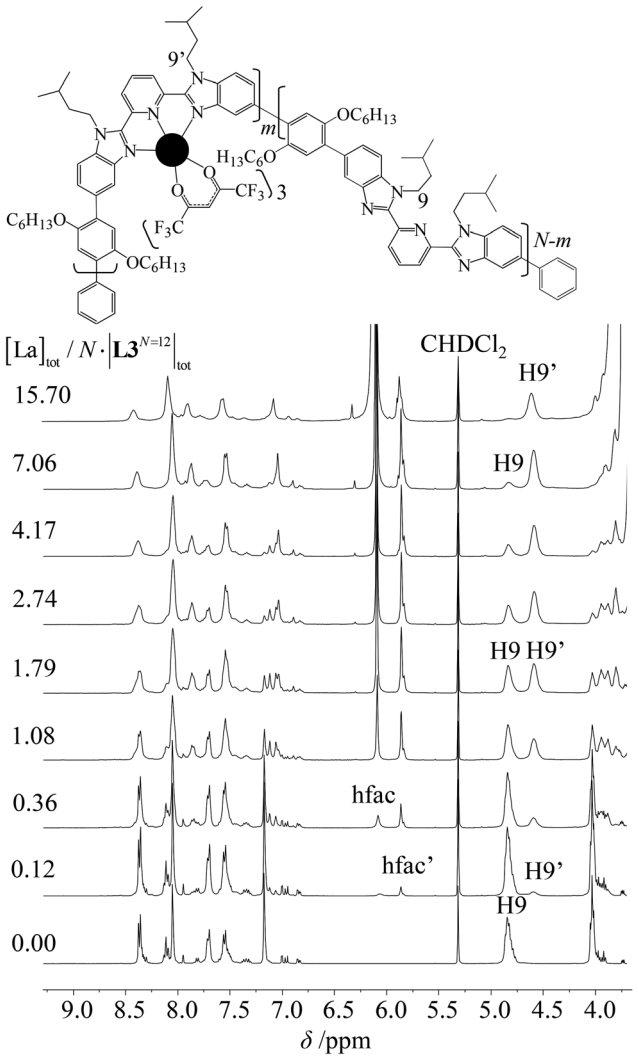

Fig. 3 ^{1}H-NMR titration of $\mathbf{L3}^{N=12}$ with [La(hfac)$_3$dig] (CD_2Cl_2 + 0.15 mol dm^{-3} diglyme at 293 K). The signal for the bound sites are designed with a single quote.

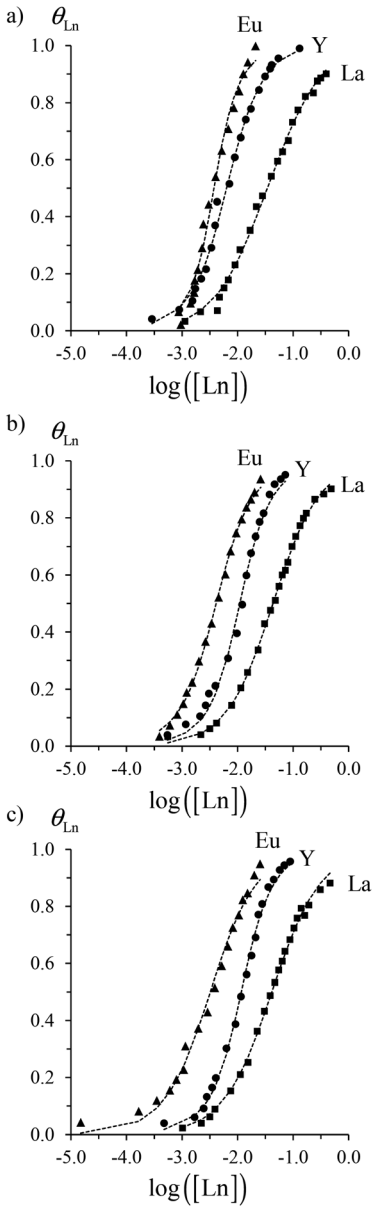

Fig. 4 Experimental occupancy factors θ_{Ln} (markers) and fitted binding isotherms using eqn (9) and (10) (dotted traces) for the titrations of (a) $\mathbf{L3}^{N=12}$ (b) $\mathbf{L3}^{N=20}$ and (c) $\mathbf{L3}^{N=31}$ with [Ln(hfac)$_3$dig] (Ln = La, Eu, Y; CD_2Cl_2 + 0.15 mol dm^{-3} diglyme at 293 K).

$$[\mathrm{Ln}] = [\mathrm{Ln}]_{\mathrm{tot}} - [\mathrm{Ln}]_{\mathrm{bound}} \quad (14)$$

$$\theta_{\mathrm{Ln}} = \frac{\langle m \rangle}{N} = \frac{1}{N}\frac{|\mathrm{Ln}|_{\mathrm{bound}}}{|\mathbf{L3}^N|_{\mathrm{tot}}} = \frac{I^{\mathrm{H}}_{\mathrm{P-Ln}}}{I^{\mathrm{H}}_{\mathrm{P}} + I^{\mathrm{H}}_{\mathrm{P-Ln}}} \quad (15)$$

As expected from previous investigations with the monomeric tridentate binding unit,[20,23] ^{19}F DOSY NMR experiments unambiguously establish the operation of the minor competitive equilibrium (16) for Ln = Eu,[28] in line with the release in solution of minor quantities of $[Ln(hfac)_4]^-$ for the smaller lanthanides (Ln = Eu in Fig. S5 and Ln = Y in Fig. S7 in the ESI†).

$$[\mathbf{L3}^N(\mathrm{Ln(hfac)_3})_m] + [\mathrm{Ln(hfac)_3dig}] \rightleftharpoons [\mathbf{L3}^N(\mathrm{Ln}_m(\mathrm{hfac})_{3_{m-1}})]^+ + [\mathrm{Ln(hfac)_4}]^- + \mathrm{dig} \quad (16)$$

Reasonably assuming that $[Ln] = [Ln(hfac)_3dig] + [Ln(hfac)_4]$ and $[Ln]_{bound} = [\mathbf{L3}^N(Ln(hfac)_3)_m] + [\mathbf{L3}^N(Ln_m(hfac)_{3_{m-1}})]$ for a global analysis of the polymer loading, the resulting binding isotherms for Ln = La, Eu and Y (Fig. 4) can be satisfyingly fitted to eqn (9) and (10) by using non-linear least squares methods to give the conditional intrinsic affinities $\Delta G^{\mathrm{Ln}}_{\mathrm{N3,cond}} = -RT(f^{\mathrm{Ln}}_{\mathrm{N3,cond}})$ and intermetallic interactions $\Delta E^{\mathrm{Ln,Ln}}_{1-2} = -RT\ln(u^{\mathrm{Ln,\,Ln}}_{1-2})$ gathered in Table 2 and graphically illustrated in Fig. 5.

Inspection of the binding isotherms immediately shows that the metal loading is strongly influenced by the size of the lanthanide (Fig. 4), whereas the length of the polymer has only minor effects (Fig. S6 in the ESI†). The bell-shaped trend found for the intrinsic affinities $\Delta G^{\mathrm{La}}_{\mathrm{N3,cond}} > \Delta G^{\mathrm{Eu}}_{\mathrm{N3,cond}} < \Delta G^{\mathrm{Y}}_{\mathrm{N3,cond}}$ along the lanthanide series (Fig. 5a) mirrors that reported for

Table 2 Thermodynamic conditional intrinsic affinities $\Delta G^{Ln}_{N3,cond} = -RT(f^{Ln}_{N3,cond})$ and intermetallic interactions $\Delta E^{Ln,Ln}_{1-2} = -RT\ln(u^{Ln,Ln}_{1-2})$ obtained by NMR titrations of $\mathbf{L3}^{N=12}$, $\mathbf{L3}^{N=20}$ and $\mathbf{L3}^{N=31}$ with [Ln(hfac)$_3$dig] (Ln = La, Eu, Y; CD_2Cl_2 + 0.15 mol dm^{-3} diglyme at 293 K)[a]

Ln	Polymer	$f^{Ln}_{N3,cond}$	$u^{Ln,Ln}_{1-2}$	$\Delta G^{Ln}_{N3,cond}$/kJ mol^{-1}	$\Delta E^{Ln,Ln}_{1-2}$/kJ mol^{-1}	AF[b]	$f_{N3}{}^{Ln\,c}$	$\Delta G^{Ln\,c}_{N3}$/kJ mol^{-1}
La	$\mathbf{L3}^{N=12}$	35.6(1.2)	0.77(3)	−8.7(1)	0.63(8)	0.034	5.3(2)	−4.08(8)
La	$\mathbf{L3}^{N=20}$	21.4(6)	1.08(3)	−7.5(1)	−0.19(6)	0.026	3.21(8)	−2.84(6)
La	$\mathbf{L3}^{N=31}$	24.5(6)	0.99(3)	−7.8(1)	0.03(6)	0.026	3.7(1)	−3.17(6)
Eu	$\mathbf{L3}^{N=12}$	132(5)	1.67(6)	−11.9(1)	−1.25(9)	0.037	19.8(7)	−7.27(9)
Eu	$\mathbf{L3}^{N=20}$	136(5)	1.83(7)	−12.0(1)	−1.47(9)	0.036	20.4(7)	−7.35(9)
Eu	$\mathbf{L3}^{N=31}$	94(4)	1.61(7)	−11.1(2)	−1.16(11)	0.045	14.1(6)	−6.45(11)
Y	$\mathbf{L3}^{N=12}$	84.3(3.7)	1.91(8)	−10.8(2)	−1.58(11)	0.044	12.6(6)	−6.18(11)
Y	$\mathbf{L3}^{N=20}$	37.4(1.7)	2.53(12)	−8.8(2)	−2.26(11)	0.046	5.6(3)	−4.20(11)
Y	$\mathbf{L3}^{N=31}$	34.5(1.5)	2.56(11)	−8.6(2)	−2.29(11)	0.044	5.2(2)	−4.00(11)

[a] The quoted uncertainties correspond to those estimated during the non-linear least-squares fits. [b] Agreement factor $AF = \sqrt{\frac{\sum_i \left(\theta^{exp}_{Ln,i} - \theta^{calcd}_{Ln,i}\right)^2}{\sum_i \left(\theta^{exp}_{Ln,i}\right)^2}}$. [c] $f^{Ln}_{N3} = f^{Ln}_{N3,\,cond} \times [dig]_{tot}$ stands for the intrinsic affinity of the ligand exchange reaction (12).

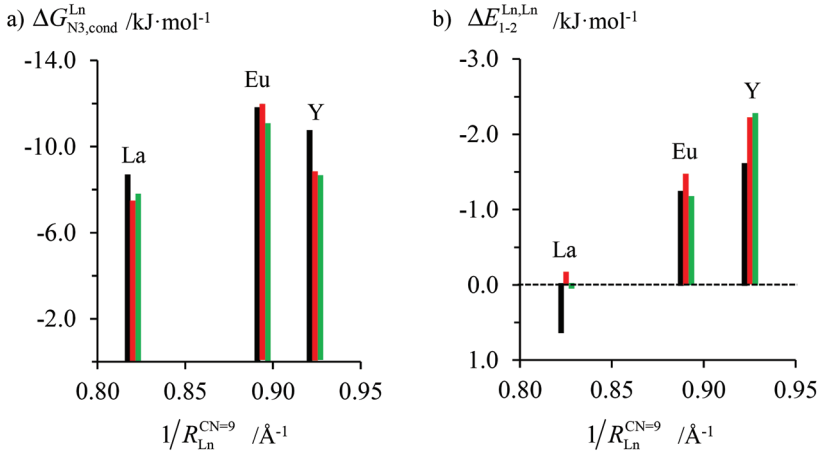

Fig. 5 Variation of the (a) intrinsic affinities $\Delta G^{Ln}_{N3,cond} = -RT(f^{Ln}_{N3,cond})$ and (b) intermetallic interactions $\Delta E^{Ln,Ln}_{1-2} = -RT\ln(u^{Ln,Ln}_{1-2})$ along the lanthanide series for the metallic loading of the three polymers $\mathbf{L3}^{N=12}$ (black), $\mathbf{L3}^{N=20}$ (red) and $\mathbf{L3}^{N=31}$ (green) *versus* the inverse of the nine-coordinate lanthanide ionic radii (CD_2Cl_2 + 0.15 mol dm^{-3} at 293 K).

the monomeric unit,[14] except for a global reduction of the absolute values by about a factor two in the polymers. Though often reported in lanthanide coordination chemistry,[29] such deviation from the standard electrostatic trends, *i.e.* a regular increase of the metal–ligand affinity with the contraction of the lanthanide ionic radius, did not find a straightforward explanation[17,30] and crystal-field effects[31] or changes in the coordination numbers of the metal around the middle of the lanthanide series[34] have been invoked. The loading process is unambiguously driven by positive cooperativity for the smaller lanthanides with $\Delta E^{Y,Y}_{1-2} < \Delta E^{Eu,Eu}_{1-2} < 0$ and statistically-controlled for the largest metal of the series ($\Delta E^{La,La}_{1-2} \approx 0$). (Fig. 5b). Again, the length of the polymers has only minor influence (Fig. 5). The latter data, collected on the monodisperse polymers of variable length $\mathbf{L3}^{N=12}$, $\mathbf{L3}^{N=20}$ and $\mathbf{L3}^{N=31}$ contrast with the uncertain and marginally positive values $0 \leq \Delta E^{Ln,Ln}_{1-2} \leq 1.4$ kJ mol^{-1} (Ln = La, Eu, Y) previously estimated from preliminary titrations using a polydisperse $\mathbf{L3}^{3\leq N\leq 18}$ sample.[35]

Dynamic light scattering analysis of the metal loading of the polymeric multi-tridentate receptors $\mathbf{L3}^N$ with [Ln(hfac)$_3$(diglyme)]

The interpretation of the neighbouring intermetallic interactions can be approached by the Born–Haber cycle depicted in Fig. 6 and summarized with eqn (17).[19] The selected complexation process refers to the addition of one lanthanide carrier [Ln(hfac)$_3$] to a [$\mathbf{L3}^N$(Ln(hfac)$_3$)$_m$] microspecies to give [$\mathbf{L3}^N$(Ln(hfac)$_3$)$_{m+1}$], in which the total intermetallic interactions increases by a single $\Delta E^{Ln,\,Ln}_{1-2}$ contribution.

$$\Delta G^{\circ}_{K_{m+1},sol} = \Delta G^{\circ}_{K_{m+1},gas} - \Delta_{solv}G^{\circ}_{\mathbf{L3}Ln_m} - \Delta_{solv}G^{\circ}_{Ln} + \Delta_{solv}G^{\circ}_{\mathbf{L3}Ln_{m+1}} \quad (17)$$

The application of the site-binding model (eqn (7) and (8)) to the K_{m+1} successive stability microconstant in the gas phase leads to $\Delta G_{K_{m+1},gas} = -RT\ln(f^{Ln}_{i,gas}) + \Delta E^{Ln,Ln}_{1-2,gas}$, where the latter intermetallic interaction $\Delta E^{Ln,\,Ln}_{1-2,gas}$ can be approximated by the interaction between two electric dipoles (eqn (18), θ is the

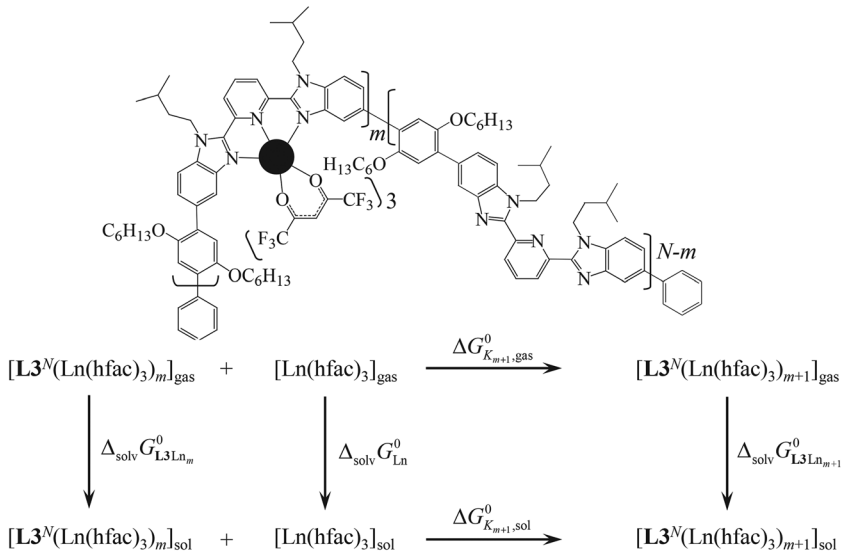

Fig. 6 Thermodynamic Born–Haber cycle for the addition of the (m + 1) [Ln(hfac)$_3$] lanthanide carrier, characterized by the K_{m+1} successive stability constant, to the lanthanidopolymer [**L3**^{N}(Ln(hfac)$_3$)$_m$].

angle between the dipole vectors)[36] produced by two adjacent [(N$_3$)Ln(hfac)$_3$] complexes (N$_3$ stands for a tridentate binding unit) separated by $R_{\mathrm{Ln-Ln}} \approx 1.2$–$1.5$ nm in the polymers **L3**^{N}.[25b] Since $\mu_{\mathrm{dip}} \leq 0.5$ Debye for Ln(hfac)$_3$ adducts,[37] eqn (18) predicts $|\Delta E^{\mathrm{Ln,Ln}}_{1-2,\mathrm{gas}}| < 20$ J mol^{-1} in vacuum with negligible variations along the lanthanide series.

$$\Delta E^{\mathrm{Ln,Ln}}_{1-2,\mathrm{gas}} = N_{\mathrm{Av}} \frac{\mu_1 \mu_2}{4\pi\varepsilon_0 \varepsilon_{\mathrm{r}}} \frac{1 - 3\cos^2\theta}{(R_{\mathrm{Ln-Ln}})^3} \tag{18}$$

The use of the Onsager eqn (5) for modelling the solvation energies $\Delta_{\mathrm{solv}}G^\circ$ transforms eqn (17) into eqn (19), where we recognize that the minor variation in size of the trivalent lanthanide $R_{\mathrm{La}} > R_{\mathrm{Eu}} > R_{\mathrm{Lu}}$ within the various tris(beta-diketonate) carriers has no significant influence. On the contrary, the changes in the global size of the polymer upon metal loading may affect the last two terms of eqn (19).

$$\Delta E^{\mathrm{Ln,Ln}}_{1-2,\mathrm{sol}} = \Delta E^{\mathrm{Ln,Ln}}_{1-2,\mathrm{gas}} - RT \ln\left(\frac{f^{\mathrm{Ln}}_{i,\mathrm{gas}}}{f^{\mathrm{Ln}}_{i,\mathrm{sol}}}\right) + \frac{N_{\mathrm{av}}}{4\pi\varepsilon_0}\left(\frac{\varepsilon_{\mathrm{r}} - 1}{2\varepsilon_{\mathrm{r}} + 1}\right) \times \left[\frac{{\mu_{\mathrm{Ln}}}^2}{(R_{\mathrm{H,Ln}})^3} + \frac{{\mu_{\mathbf{L3}\mathrm{Ln}_m}}^2}{(R_{\mathrm{H},\mathbf{L3}\mathrm{Ln}_m})^3} - \frac{{\mu_{\mathbf{L3}\mathrm{Ln}_{m+1}}}^2}{(R_{\mathrm{H},\mathbf{L3}\mathrm{Ln}_{m+1}})^3}\right] \tag{19}$$

In this context, it is well-known that the meridional complexation of the tridentate 2,6-bis(benzimidazol-2-yl)pyridine binding units found in the polymers **L3**^{N} is accompanied by a drastic structural change from a linear *trans–trans* conformation in the free site (right part of the structure in Fig. 6) toward a bent *cis–cis* conformation in its cooordinate counterpart (left part of the structure in Fig. 6).[38] The repetition of this structural change upon successive metal loading affects the global geometries and sizes of the lanthanidopolymers [**L3**^{N}(Ln(hfac)$_3$)$_m$]. NMR DOSY experiments in absence of high-gradient fields are not accurate enough to detect the latter size variations in the lanthanidopolymers, but DLS measurements perfomed during the titration of **L3**^{N} with [Ln(hfac)$_3$dig] in dichloromethane indeed provided the reliable hydrodynamic diameters as depicted in Fig. 7 and Fig. S9 and S10 (ESI†).

We observe a monotonous increase in hydrodynamic diameters from **L3**^{N} = 12 (3.9(2) nm, Fig. S9†) to **L3**$^{N=20}$ (4.7(1) nm, Fig. 7) and **L3**$^{N=31}$ (6.1(2) nm, Fig. S10†), which can be analyzed within the framework of Kuhn theory for a Gaussian chain summarized in eqn (20), where R_{H} is the hydrodynamic radius, R_{ee} is the end-to-end distance of the polymer considered as a flexible chain made up of rigid segments of Kuhn length l, l_0 = 1.56 nm is the length of the monomer measured in its crystal structure[14] and N is the number of monomers, *i.e.* the degree of polymerization in **L3**^{N}.[32,33]

$$R_{\mathrm{H}} = \sqrt{\frac{3\pi}{128}} R_{\mathrm{ee}} = \sqrt{\frac{3\pi}{128}} \sqrt{l l_0 N} = \sqrt{\frac{3\pi l l_0}{128}} \sqrt{N} \tag{20}$$

Despite the relatively low number of monomers, the plot of R_{H} *versus* N displayed the expected square root dependence for a Gaussian chain (Fig. S11†), from which a Kuhn length of l = 2.58(7) nm can be estimated. Our polymers **L3**^{N} are relatively flexible, since the Kuhn length is comparable to the monomer length. This flexibility can be explained by the large monomer unit. However, the most important point concerns the global invariance of the size of the [**L3**^{N}(Ln(hfac)$_3$)$_m$] polymers upon loading with mid-range Ln = Eu (Fig. 7b, S9b and S10b†), whereas the use of a smaller cation Ln = Y leads to contraction (Fig. 7c, S98c and S10c†) while a larger cation Ln = La (Fig. 7a, S9a and S10a†) produces an upward concave trace diagnostic for an overall size increase. The introduction of these trends into eqn (19) predicts that the decrease in size observed upon the successive complexation of the smaller lanthanides (Ln = Eu, = Y), *i.e.* $R_{\mathrm{H},\mathbf{L3}\mathrm{Ln}_{m+1}} < R_{\mathrm{H},\mathbf{L3}\mathrm{Ln}_m}$ favours

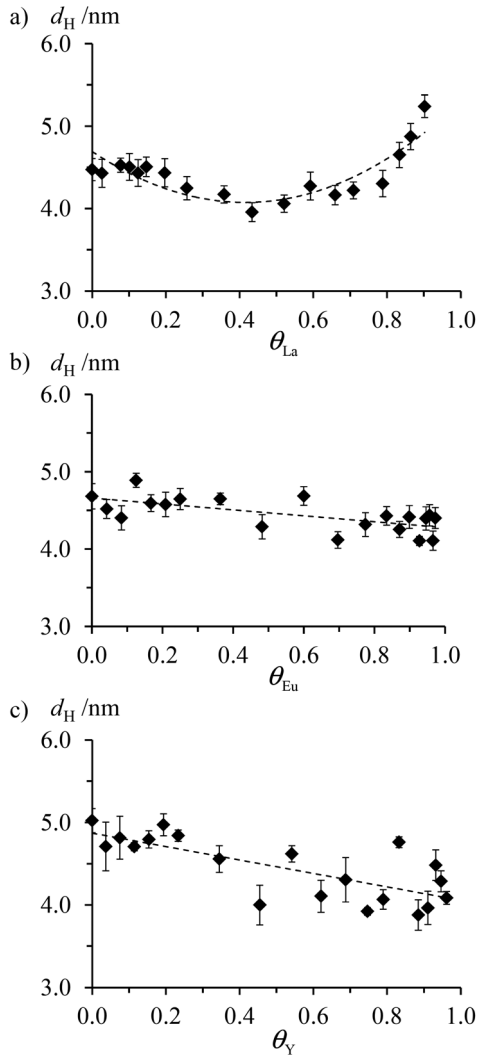

Fig. 7 Hydrodynamic diameters for the lanthanidopolymers [**L3**$^{N=20}$(Ln(hfac)$_3$)$_m$] as a function of the occupancy factor θ_{Ln} for lanthanide loadings with (a) [La(hfac)$_3$dig], (b) [Eu(hfac)$_3$dig] and (c) [Y(hfac)$_3$dig] (CH_2Cl_2 + 0.15 mol dm^{-3} diglyme at 293 K). The trendlines are only guides for the eyes.

positive cooperativity ($\Delta E^{Ln,Ln}_{1-2,sol} < 0$), while the increase in size found Ln = La promotes anti-coperativity ($\Delta E^{Ln,Ln}_{1-2,sol} > 0$). The experimental results $0 \approx \Delta E^{La,La}_{1-2,sol} < \Delta E^{Eu,Eu}_{1-2,sol} < \Delta E^{Y,Y}_{1-2,sol}$ (Fig. 5b) fairly match this trend whatever the length of the receptors.

Conclusion

The optimization of the Suzuki coupling reactions between the tridentate binding units **1** and the lipophilic bridges **2** provides close to monodisperse polymers of various length **L3**^{N} (N = 10–30), the distribution of which is compatible with the thermodynamic and structural investigation of their metal loading in solution with the help of NMR and light scattering titrations. In line with the monomer, the non-cooperative intrinsic thermodynamic affinity of each tridentate site in the polymer for the entering lanthanide carrier, Ln(hfac)$_3$, display a bell-shaped trend with a maximum avidity for mid-sized lanthanides. However, the nearest-neighbour intermetallic interactions unambiguously point to an increase of the affinity of the binding sites for successive loadings with small lanthanides (positive cooperativity), whereas Ln = La, the largest metal of the series, exhibits roughly statistical behaviour. The length of the polymer has little, if any, influence on the lanthanide loading. Dynamic light scattering measurements indicate that (i) the lanthanidopolymers show no trend towards aggregation and (ii) positive cooperativity is correlated with the contraction of the polymer upon metal loading, an effect assigned to solvation effects. Though modest in term of absolute magnitude and comparable with thermal energy ($RT \approx 2.5$ kJ mol^{-1} at room temperature), the attractive intermetallic interactions $\Delta E^{Eu,Eu}_{1-2,sol} < 0$ and $\Delta E^{Y,Y}_{1-2,sol} < 0$ measured in **L3**^{N} do not produce exploitable metal clustering, but they pave the way for producing larger effects by simply increasing the local dipole moments of the lanthanide carriers which contribute to the solvation effects *via* the square of their norms. The use of unsymmetrical beta-diketonate in the lanthanide carriers is known to increase the dipole moment by at least one order of magnitude,[37] and therefore both intermetallic gas-phase interactions (eqn (18)) and solvation energies (eqn (5)) might be modified by two or more orders of magnitude.

Experimental

Solvents and starting materials

These were purchased from Strem, Acros, Fluka AG and Aldrich and used without further purification unless otherwise stated. 2,6-Bis-[1-(3-methylbutyl)-5-bromo-benzomidazol-2-yl)-pyridine (**1**)[23] and 2,5-dihexyloxy-1,4-diboronic acid (**2**)[24] were prepared according to literature procedures. The hexafluoroacetylacetonate salts [Ln(hfac)$_3$(diglyme)] were prepared from the corresponding oxide (Aldrich, 99.99%).[26] Acetonitrile and dichloromethane were distilled over calcium hydride.

Preparation of polymers L3$^{N=12}$ and L3$^{N=20}$. 2,6-Bis-[1-(3-methylbutyl)-5-bromo-benzomidazol-2-yl)pyridine (**1**, 3 g, 4.9 mmol), 2,5-dihexyloxy-1,4-diboronic acid (**2**, 1.8 g, 4.9 mmol) and CsF (4.5 g, 29.4 mmol) were dissolved in degassed dioxane/EtOH (3/1, 120 mL). The solution was saturated with argon for 30 min before adding Pd(PPh$_3$)$_4$ (566 mg, 0.49 mmol, 10 equiv.). The reaction mixture was stirred under argon at 80 °C for 3 days. The polymerization was completed with the addition of bromobenzene (769.3 mg, 4.9 mmol, 1 equiv.), followed 24 h later with the addition of phenylboronic acid (600 mg, 4.9 mmol, 1 equiv.). The final mixture was stirred for 24 h at 80 °C, and the solvents were removed under vacuum. The residue was dissolved in chloroform (300 mL), and the organic phase successively washed with brine (3 × 100 mL) and water (150 mL). The organic layer was dried (Na_2SO_4), filtered and evaporated to dryness. The solid was dissolved in a minimum amount of chloroform, then poured

dropwise into methanol (800 mL) to give a pale brown solid (2.23 g, M_w = 12 924 g mol^{-1}, I_p = 1.31, Fig. S12, ESI†). This process was repeated to yield 1.59 g of polymer (M_w = 12 630 g mol^{-1}, I_p = 1.22, Fig. S12†). The latter solid was dissolved in 50 ml of chloroform, and methanol was dropwise added (reverse precipitation) until an important quantity of solid was obtained, filtered and dried under vacuum (1.30 g, M_w = 11 539 g mol^{-1}, I_p = 1.13, Fig. S12†). The process of reverse precipitation was repeated to give **L3**$^{N=20}$ (835 mg, M_w = 14 759 g mol^{-1} , I_p = 1.16, Fig. S12†). The filtrate was evaporated and dried under a vacuum to yield **L3**$^{N=12}$ (320 mg, M_w = 8743 g mol^{-1} , I_p = 1.13, Fig. S12†).

Preparation of polymer L3$^{N=31}$. 2,6-Bis-[1-(3-methylbutyl)-5-bromo-benzomidazol-2-yl)pyridine (**1**, 1 g, 1.63 mmol), 2,5-dihexyloxy-1,4-diboronic acid (**2**, 600.7 mg, 1.63 mmol) and CsF (2.59 g, 16.6 mmol) were dissolved in degassed tolene/ethanol (3/1, 20 mL). The solution was saturated with argon for 30 min before adding $Pd(PPh_3)_4$ (188.7 mg, 1.63 mmol, 10 equiv.). The reaction mixture was then stirred under argon at 80 °C for 3 days. The polymerization was completed with the addition of bromobenzene (256.4 mg, 1.63 mmol, 1 equiv.), followed 24 h later with the addition of phenylboronic acid (203.7 mg, 1.63 mmol, 1 equiv.). The final mixture was stirred for 24 h at 80 °C, and the solvents were removed. The residue was dissolved in chloroform (200 mL), and the organic phase successively washed with brine (3 × 100 mL) and water (150 mL). The organic layer was dried (Na_2SO_4), filtered, and evaporated to dryness. The solid was dissolved in a minimum amount of chloroform, and then poured dropwise into methanol (500 mL). The pale brown solid was filtred and again dissolved in chloroform, then poured dropwise into methanol. Centrifugation followed by decantation and drying gave **L3**$^{N=31}$ (235 mg, M_w = 22 456 g mol^{-1}, I_p = 1.248) as a pale brown solid.

Spectroscopic measurements

^{1}H, ^{19}F and ^{13}C NMR spectra were recorded at 293 K on a Bruker Avance 400 MHz spectrometer. Chemical shifts are given in ppm with respect to TMS (^{1}H) or C_6F_6 (^{19}F). DOSY-NMR data used the pulse sequence implemented in the Bruker program *ledbpgp2s*[39] which employed stimulated echo, bipolar gradients and longitudinal eddy current delay as the *z* filter. The four 2 ms gradient pulses had sine-bell shapes and amplitudes ranging linearly from 2.5 to 50 G cm^{-1} in 32 steps. The diffusion delay was in the range 60–140 ms depending on the analyte diffusion coefficient, and the number of scans was 32. The processing was done using a line broadening of 5 Hz and the diffusion coefficients were calculated with the Bruker processing package.

Gel permeation chromatography (GPC)

The absolute molecular weights of the polymer were determined from THF solution at 303 K by using a Viscotek TDAmax quadruple detectors array incorporating refractive index, light scattering, viscosimeter and UV detectors.

Static and dynamic light scattering measurements

Light scattering measurements were performed at a scattering angle of 173° with the Zetasizer ZS (Malvern Instruments) at a wavelength of 633 nm. The molecular weight M_w was determined by SLS means of the relation $KC/R = 1/M_w$ where C was the mass concentration, R the Rayleigh ratio, and K an optical constant. The scattering intensity of the sample, from which the solvent contribution was subtracted, was converted to the Rayleigh ratio by means of the scattering intensity of toluene and its known Rayleigh ratio.[40] Due to the low molecular weight of the polymers, any contributions from the form factor at the scattering angle used could be neglected. The concentrations of 1–3 g L^{-1} used were sufficiently small, such that contributions from polymer–polymer interactions were negligible. The refractive index increment (Fig. S2†), which was needed to obtain the optical constant, was measured with a refractometer (Abbemat, Anton Paar) at the same wavelength. DLS was carried out at concentrations of 3 g L^{-1} and the hydrodynamic diameter was extracted by second order cumulant analysis and using the respective viscosities of the solvent.

Acknowledgements

Financial support from the Swiss National Science Foundation is gratefully acknowledged. ZW thanks the program of China Scholarship Council (no. 2011842681) for financial support.

References

1 (*a*) M. O. Wolf, *Adv. Mater.*, 2001, **13**, 545; (*b*) M. O. Wolf, *J. Inorg. Organomet. Polym.*, 2006, **16**, 189.
2 (*a*) G. Koper and M. Borkovec, *J. Phys. Chem. B*, 2001, **105**, 6666; (*b*) M. Borkovec, G. J. M. Koper and C. Piguet, *Curr. Opin. Colloid Interface Sci.*, 2006, **11**, 280; (*c*) G. J. M. Koper and M. Borkovec, *Polymer*, 2010, **51**, 5649.
3 M. Borkovec, J. Hamacek and C. Piguet, *Dalton Trans.*, 2004, 4096.
4 G. Ercolani and L. Schiaffino, *Angew. Chem., Int. Ed.*, 2011, **50**, 1762–1768.
5 (*a*) A. Adronov and J. M. J. Fréchet, *Chem. Commun.*, 2000, 1701; (*b*) M. Kawa and T. Takahagi, *Chem. Mater.*, 2004, **16**, 2282; (*c*) J. P. Cross, M. Lauz, P. D. Badger and S. Petoud, *J. Am. Chem. Soc.*, 2004, **126**, 16278; (*d*) B. Branchi, P. Ceroni, V. Balzani, F.-G. Klärner and F. Vögtle, *Chem. – Eur. J.*, 2010, **16**, 6048; (*e*) A. Foucault-Collet, C. M. Shade, I. Nazarenko, S. Petoud and S. V. Eliseeva, *Angew. Chem., Int. Ed.*, 2014, **53**, 2927.
6 (*a*) J. B. Oh, Y. H. Kim, M. K. Nah and H. K. Kim, *J. Lumin.*, 2005, **111**, 255; (*b*) A. Nonat, M. Regueiro-Figueroa, D. Esteban-Gomez, A. de Blas, T. Rodriguez-Blas, C. Platas-Iglesias and L. J. Charbonnière, *Chem. – Eur. J.*, 2012, **18**, 8163; (*c*) A. Zaïm, S. V. Eliseeva, L. Guénée, H. Nozary, S. Petoud and C. Piguet, *Chem. – Eur. J.*, 2014, **20**, 12172.

7 (*a*) D. R. Kauffman, C. M. Shade, H. Uh, S. Petoud and A. Star, *Nat. Chem.*, 2009, **1**, 500; (*b*) J. An, C. M. Shade, D. A. Chengelis-Czegan, S. Petoud and N. L. Rosi, *J. Am. Chem. Soc.*, 2011, **133**, 1220.

8 (*a*) H. Tsukube and S. Shinoda, *Chem. Rev.*, 2002, **102**, 2389; (*b*) S. Pandya, J. Yu and D. Parker, *Dalton Trans.*, 2006, 2757; (*c*) Y. Cui, Y. Yue, G. Qian and B. Chen, *Chem. Rev.*, 2012, **112**, 1126–1162; (*d*) S. J. Bradberry, A. J. Savyasachi, M. Martinez-Calvo and T. Gunnlaugsson, *Coord. Chem. Rev.*, 2014, **273–274**, 226; (*e*) M. C. Heffern, L. M. Matosziuk and T. J. Meade, *Chem. Rev.*, 2014, **114**, 4496–4539.

9 (*a*) F. Auzel, *Chem. Rev.*, 2004, **104**, 139; (*b*) B. M. van der Ende, L. Aarts and A. Meijerink, *Phys. Chem. Chem. Phys.*, 2009, **11**, 11081; (*c*) S. Han, R. Deng and X. Liu, *Angew. Chem., Int. Ed.*, 2014, **53**, 11702; (*d*) S. Gai, C. Li, P. Yang and J. Lin, *Chem. Rev.*, 2014, **114**, 2343; (*e*) G. Chem, H. Qiu, P. N. Prasad and X. Chen, *Chem. Rev.*, 2014, **114**, 5161.

10 (*a*) N. Dalla Favera, J. Hamacek, M. Borkovec, D. Jeannerat, G. Ercolani and C. Piguet, *Inorg. Chem.*, 2007, **46**, 9312; (*b*) C. Piguet and J.-C. G. Bünzli, in *Handbook on the Physics and Chemistry of Rare Earths*, ed. K. A. Gschneidner Jr., J.-C. G. Bünzli and V. K. Pecharsky, Elsevier Science, Amsterdam, 2010, vol. 40, pp. 301–553.

11 J. M. Stanley and B. J. Holliday, *Coord. Chem. Rev.*, 2012, **256**, 1520.

12 J. K. Mwaura, D. L. Thomsen III, T. Phely-Bobin, M. Taher, S. Theodoropulos and F. Papadimitrakopoulos, *J. Am. Chem. Soc.*, 2000, **122**, 2647.

13 B. M. McKenzie, R. J. Wojtecki, K. A. Burke, C. Zhang, A. Jakli, P. T. Mather and S. J. Rowan, *Chem. Mater.*, 2011, **23**, 3525.

14 L. Babel, T. N. Y. Hoang, H. Nozary, J. Salamanca, L. Guénée and C. Piguet, *Inorg. Chem.*, 2014, **53**, 3568.

15 T. Dutronc, E. Terazzi and C. Piguet, *RSC Adv.*, 2014, **4**, 15740.

16 B. M. Castellano and D. K. Eggers, *J. Phys. Chem. B*, 2013, **117**, 8180.

17 (*a*) G. R. Choppin, in *Lanthanide Probes in Life, Chemical and Earth Science*, ed. J.-C. G. Bünzli and G. R. Choppin, Elsevier, Amsterdam, 1989, pp. 1–42; (*b*) G. R. Choppin and E. N. Rizkalla, in *Handbook on the Physics and Chemistry of Rare Earths*, ed. K. A. Gschneidner Jr., L. Eyring, G. R. Choppin and G. H. Lander, Elsevier Science B. V., 1994, vol. 18, pp. 559.

18 N. Dalla Favera, U. Kiehne, J. Bunzen, S. Hyteballe, A. Lützen and C. Piguet, *Angew. Chem., Int. Ed.*, 2010, **49**, 125.

19 T. Riis-Johannessen, N. Dalla Favera, T. K. Todorova, S. M. Huber, L. Gagliardi and C. Piguet, *Chem. – Eur. J.*, 2009, **15**, 12702.

20 A. Zaïm, N. Dalla Favera, L. Guénée, H. Nozary, T. N. Y. Hoang, S. V. Eliseeva, S. Petoud and C. Piguet, *Chem. Sci.*, 2013, **4**, 1125.

21 (*a*) M. Born, *Zeit. Phys.*, 1920, **1**, 45; (*b*) R. H. Stokes, *J. Am. Chem. Soc.*, 1964, **86**, 979; (*c*) A. Kumar, *J. Phys. Soc. Jpn.*, 1992, **61**, 4247–4250.

22 (*a*) L. Onsager, *J. Am. Chem. Soc.*, 1936, **58**, 1486; (*b*) D. V. Matyushov, *J. Chem. Phys.*, 2004, **120**, 1375; (*c*) C. J. Cramer and D. G. Truhlar, *Acc. Chem. Res.*, 2008, **41**, 760–768.

23 A. Zaïm, H. Nozary, L. Guénée, C. Besnard, J.-F. Lemonnier, S. Petoud and C. Piguet, *Chem. – Eur. J.*, 2012, **18**, 7155.

24 C.-J. J. Wu, C. Xue, Y.-M. Kuoa and F.-T. Luob, *Tetrahedron*, 2005, **61**, 4735.

25 (*a*) J.-F. Lemonnier, L. Guénée, G. Bernardinelli, J.-F. Vigier, B. Bocquet and C. Piguet, *Inorg. Chem.*, 2010, **49**, 1252; (*b*) J.-F. Lemonnier, L. Guénée, C. Beuchat, T. A. Wesolowski, P. Mukherjee, D. H. Waldeck, K. A. Gogik, S. Petoud and C. Piguet, *J. Am. Chem. Soc.*, 2011, **133**, 16219.

26 (*a*) W. J. Evans, D. G. Giarikos, M. A. Johnston, M. A. Greci and J. W. Ziller, *J. Chem. Soc., Dalton Trans.*, 2002, 520; (*b*) G. Malandrino, R. Lo Nigro, I. L. Fragalà and C. Benelli, *Eur. J. Inorg. Chem.*, 2004, 500.

27 For ^{19}F-NMR titration, the integrations of the signals refer to the concentrations of free (I^{F}_{Ln}) and bound (I^{F}_{P-Ln}) metal, instead of those of free and bound sites obtained by ^{1}H-NMR. Eqn (13)–(15) must be replaced with $[Ln] = [Ln]_{tot} - [Ln]_{bound} = \left(\frac{I^{F}_{Ln}}{I^{F}_{Ln} + I^{F}_{P-Ln}}\right)[Ln]_{tot}$ and $\theta_{Ln} = \frac{\langle m \rangle}{N} = \frac{1}{N}\frac{|Ln|_{bound}}{|\mathbf{L3}^{N}|_{tot}} = \left(\frac{I^{F}_{P-Ln}}{I^{F}_{Ln} + I^{F}_{P-Ln}}\right)\frac{|Ln|_{tot}}{N|\mathbf{L3}^{N}|_{tot}}$.

28 The experimental diffusion coefficients obtained in CD_2Cl_2 + 0.15 mol dm^{-3} diglyme at 293 K are $D = 5.3(2) \times 10^{-10}$ m^2 s^{-1} for $[Eu(hfac)_4]^-$, $D = 4.7(5) \times 10^{-10}$ m^2 s^{-1} for $[Eu(hfac)_3dig]$ and $D = 1.6(2) \times 10^{-10}$ m^2 s^{-1} for $[\mathbf{L3}^{N=12}(Eu(hfac)_3)_m]$.

29 (*a*) V. S. Sastri, J.-C. G. Bünzli, V. Ramachandra Rao, G. V. S. Rayudu and J. R. Perumareddi, *Modern Aspects of Rare Earths and Their Complexes*, Elsevier B. V., Amsterdam, 2003; (*b*) P. Di Bernardo, A. Melchior, M. Tolazzi and P. L. Zanonato, *Coord. Chem. Rev.*, 2012, **256**, 328; (*c*) P. J. Panak and A. Geist, *Chem. Rev.*, 2013, **113**, 1199.

30 L. C. Thompson, Complexes, in *Handbook on the Physics and Chemistry of Rare Earths*, ed. K. A. Gschneidner Jr. and L. Eyring, North-Holland Publishing Company, 1979, vol. 3, pp. 209–297.

31 K. B. Yatsimirskii and N. A. Kostromina, *Zh. Neorg. Khim.*, 1964, **9**, 1793.

32 W. Kuhn, *Kolloid Z.*, 1934, **68**, 2.

33 I. Teraoka, *Polymer Solutions*, John Wiley & Sons Inc., New York, 2002.

34 (*a*) N. Kaltsoyannis and P. Scott, *The f Elements*, Oxford Science Publication, Oxford, 1999; (*b*) L. Helm and A. E. Merbach, *Chem. Rev.*, 2005, **105**, 1923.

35 In ref. 14, the preliminary thermodynamic analysis of the lanthanide loading of the polydisperse $\mathbf{L3}^{3\leq N\leq 18}$ polymer neglected (i) partial dissociation of hfac anions (eqn (17)) and (ii) the presence of 19% of inactive material in the sample. A careful re-examination of the corrected binding isotherm in Fig. S8 in the ESI† gives $\Delta G^{Eu}_{N3,cond} = -RT(\beta^{Eu}_{N3,cond}) = -12.1$ kJ mol^{-1} and $\Delta G^{Eu,Eu}_{1-2} = -RT\ln(u^{Eu,Eu}_{1-2}) = -1.2$ kJ mol^{-1} in line

with the data collected on the monodisperse polymers **L3**$^{N=12}$, **L3**$^{N=20}$ and **L3**$^{N=31}$.

36 P. Atkins and J. De Paula, *Physical Chemistry*, W. H. Freeman and Company, New York, 9th edn, 2010, p. 634.

37 A. Y. Rogachev, A. V. Nemukhin, N. P. Kuzmina and D. V. Sevastyanov, *Dodlaky Chem.*, 2003, **389**, 87.

38 (*a*) A. Escande, L. Guénée, K.-L. Buchwalder and C. Piguet, *Inorg. Chem.*, 2009, **48**, 1132; (*b*) C. Piguet and J.-C. G. Bünzli, *Handbook on the Physics and Chemistry of Rare Earths*, ed. K. A. Gschneidner Jr., J.-C. G. Bünzli and V. K. Pecharsky, Elsevier Science B. V., 2010, vol. 40, pp. 301–553.

39 D. Wu, A. Chen and C. S. Johnson Jr., *J. Magn. Reson., Ser. A*, 1995, **115**, 260.

40 (*a*) P. Debye, *J. Appl. Phys.*, 1944, **15**, 338; (*b*) *Neutrons, X-rays and Light. Scattering Methods Applied to Soft Condensed Matter*, ed. P. Lindner and T. Zemb, Elsevier, North Holland, 2002.